

Automating differential photometry of Intermediate Polars to study and quantify their low-flux states

Ben Pearson

May 10, 2022

Contents

1 Acknowledgements	2
2 Abstract	3
3 Introduction	3
4 Observation Setup	7
4.1 Targets	7
4.2 Differential photometry	8
4.3 Relevant technologies	8
4.4 Program	9
4.4.1 Program constants and directory structure	9
4.4.2 Indexing directories <code>index_dir</code>	10
4.4.3 Finding the best calibration files <code>find_dark</code> and <code>find_flat</code>	10
4.4.4 Photometry Function <code>run_photometry</code>	10
4.4.5 Plotting <code>plot_light_curve</code>	11
4.4.6 Cron job and Run Script	12
5 Results	12
5.1 Data	12
5.2 Analysis	13
5.3 Summary and Conclusions	14
6 Appendix A: Annotated plots	16

1 Acknowledgements

Thank you to my thesis mentor Prof. Richard Plotkin and his postdoctoral researcher Dr. Aarran Shaw for their guidance throughout this project, and my mother Crystal Lewis-Pearson for assistance in proofreading this paper.

2 Abstract

Intermediate polars are systems consisting of a main sequence “donor” star and an accreting white dwarf with a strong magnetic field ($B \leq 5 \times 10^6 G$). To further understand Intermediate polars and their recently discovered “dips” in luminosity, Dr. Aarran Shaw aims to gather pointed X-ray observations. To determine the optimal timing of such observations a visible range telescope, the Great Basin Observatory, was used to observe dips in the V filter of 13 target stars. From March 2020 to April 2022, 9 dips were found among the 13 target stars. To assist with the calibration and analysis of this data, a program was written to generate new light curves of each target daily.

3 Introduction

In cosmology, the study of the nature and age of the universe, having a foundation from which to make observations is one of the most fundamental challenges. As our instruments for observing the sky have improved, so has our ability to measure distances using parallax, or to measure the luminosity of a star. However, with distant observations we are not able to take advantage of these techniques to the same precision - thus we need another source. This is the motivation for finding what astronomers refer to as the “standard candle,” which is a star or event that has a very predictable luminosity regardless of its location relative to earth or the conditions in its galactic neighborhood. One of the most important “standard candles” is the Type 1a Supernova (sometimes referred to as the “standard candle” supernova) which is the result of an exploding white dwarf (WD) (Laboratory, 2014).

WDs are stellar core remnants, generally formed from stars of about $2M_{\odot}$ resulting in WDs of about $0.6M_{\odot}$ (Maoz, 2016, page 81). WDs are formed when stars run out of fusion material and thus lose their ability to maintain the outward pressure required to maintain hydrostatic equilibrium. As such, the core begins to collapse until it is compact enough for electron degeneracy pressure to re-establish hydrostatic equilibrium. Because of shrinkage during the process, WDs tend to be extremely hot, and as such, their emissions peak in the ultraviolet (UV) range with some emitting soft X-rays (Maoz, 2016).

Cataclysmic variables (CVs) are stars that irregularly modulate in brightness - typically between a normal phase and a dip or spike in luminosity. Generally, they consist of a main sequence “donor” star orbiting and shedding material, about a WD. WDs in cataclysmic variables tend to have higher masses than typical WDs, peaking around $0.83 \pm 0.19M_{\odot}$ (Maoz, 2016), though exactly why is not yet clear. The first proposed explanation is that more massive stars are more likely to form CVs. This would imply a starting mass of $4.0 \pm 1.7M_{\odot}$ (Maoz, 2016, page 81). Another proposed explanation posits that the increased mass is a result of accreting material.

Polars are a subclass of CVs in which the WD is extremely magnetic. Their strong mag-

netic fields prevent an accretion disk from forming causing shedded material to form a channel flowing towards the poles of the WD. This causes the orbital period of the donor star (P_{orb}) and the spin period of the WD (P_{spin}) to synchronize. Intermediate polars (IPs) have comparatively weaker magnetic fields ($B \leq 5 \times 10^6 G$) which disrupt the interior regions of the accretion disk of WDs making the accreting matter of the disk flow along the magnetic field lines towards the poles of the WD, figure 1 shows an artistic impression of this process. As a result of the lower magnetic field, IPs have an unsynchronized orbital period and spin period. This can be seen through the power spectra where the orbital frequency ($\Omega = \frac{1}{P_{orb}}$), the WD spin frequency ($\omega = \frac{1}{P_{spin}}$), and their beat frequency ($\omega - \Omega$) and associated harmonics dominate (Covington et al., 2021). For a spectrum analysis and breakdown of dominating harmonics, see figure 2.

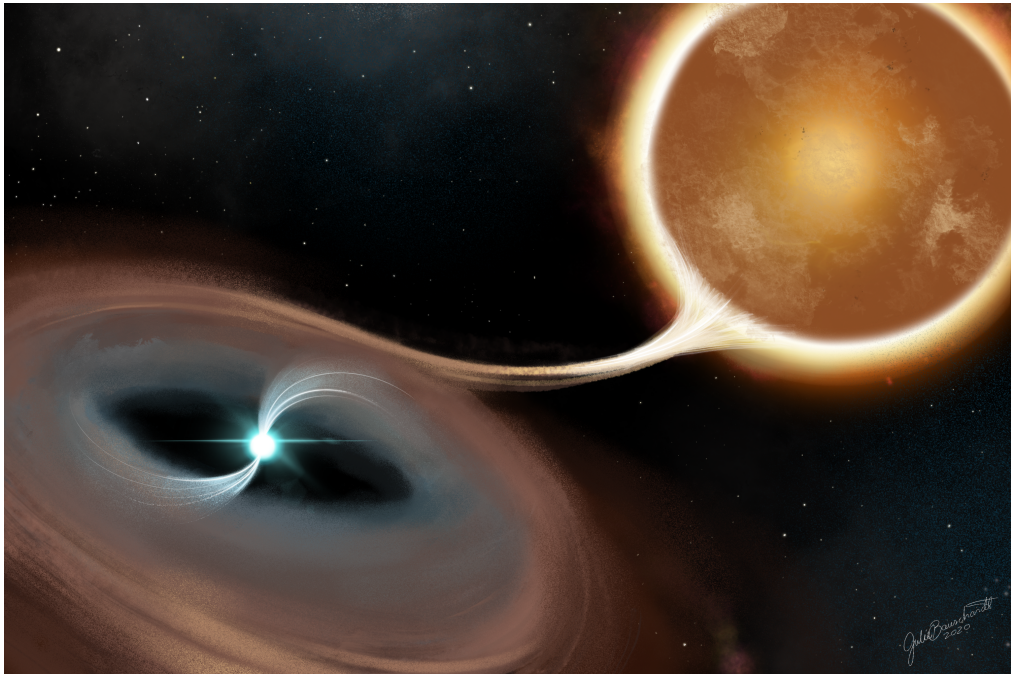


Figure 1: Artistic depiction of Magnetic Cataclysmic Variable accreting material, Image Credit: Julie Bauschardt

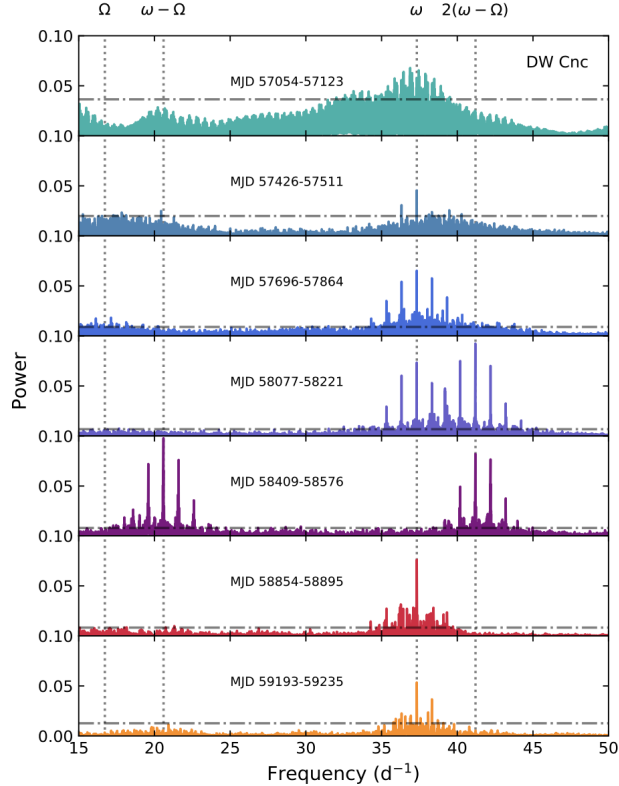


Figure 2: Lomb-Scargle periodograms of the CV -band light curves of DW Cnc. Colors match periods referenced in fig 4 with dotted vertical lines indicating known periodicities (Covington et al., 2021).

As of 2018, 70 IPs and roughly 130 polars had been found. These IPs were primarily identified in the hard X-ray band ($> 20\text{keV}$) whereas only 13 of the 130 polars were identified in the hard X-ray band (Falanga et al., 2018). These X-rays are primarily formed by the WDs themselves and their accretion disks. As the accreting material falls towards the WD it heats up and radiates. Hence, the closer to the WD the material is, the hotter it is and the more powerful the radiation.

Understanding the X-ray emissions of CVs is vital to further understanding them as the innermost regions of the accretion flow close to the surface of the WD are strongly dominated by X-rays. As matter falls towards the WD, its gravitational potential energy is converted into kinetic energy, and as it collides with more material it will heat up and radiate as a black body at extreme temperatures. For an accreting WD, the temperature at any given radius can be found through equation 1 (Maoz, 2016, page 102).

$$T(r) = \left(\frac{GM\dot{M}}{8\pi\sigma} \right)^{1/4} r^{-3/4} \quad (1)$$

Then, for a WD on the order of $1M_{\odot}$ a radius of 10^4 km, and an accretion rate of $10^{-9}M_{\odot}/\text{yr}$, at the inner radius the resulting temperature is $T = 5 \times 10^4 K$ (Maoz, 2016, page 104). This would peak in the far ultraviolet and is only about ten times hotter than the surface of the Sun

(Williams, n.d.). The hard X-rays that these observations are designed for are a result of the further infalling matter as seen in figure 3.

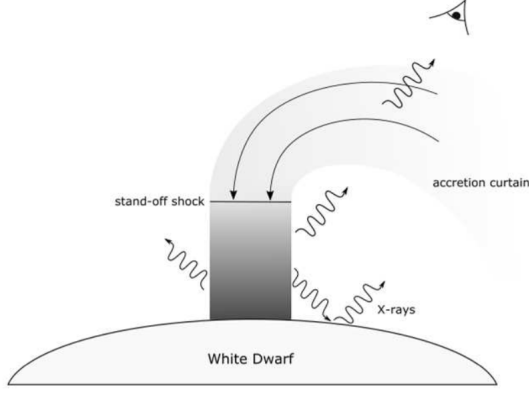


Figure 3: Diagram of infalling matter as the source of hard X-rays from Intermediate polars (Hailey et al., 2016)

As the infalling matter approaches the inner disk, it begins to follow the magnetic field lines of the WD until colliding with the WD where it forms a standing shock. This converts the kinetic energy into thermal energy and produces hard X-rays in the post-shock region. The temperature of this area can be modeled with equation 2 (Suleimanov et al., 2019)

$$kT_{sh} = \frac{3}{16}\mu m_p v_{ff}^2 \quad (2)$$

Where T_{sh} is the temperature of the material, k is the Boltzmann constant, μ is the mean molecular weight of ionized plasma, and m_p is the mass of a proton. The temperature of the infalling material is dependent upon its velocity, which is modeled by equation 3

$$v_{ff}^2 = 2GM \left(\frac{1}{R + H_{sh}} - \frac{1}{R_m} \right) \quad (3)$$

Where G is the gravitational constant, M is the mass of the WD, R is the radius of the WD and R_m is the magnetospheric radius (Suleimanov et al., 2019).

In recent years IPs have been found to undergo irregular dips in brightness. Previously unanticipated, these “low states” correspond to a decrease in the rate of accretion of the WD. Examples of such low states can be seen in figure 4. Covington et al. were able to congregate data from the American Association of Variable Star Observers (AAVSO) to observe light curves as seen in figure 4.

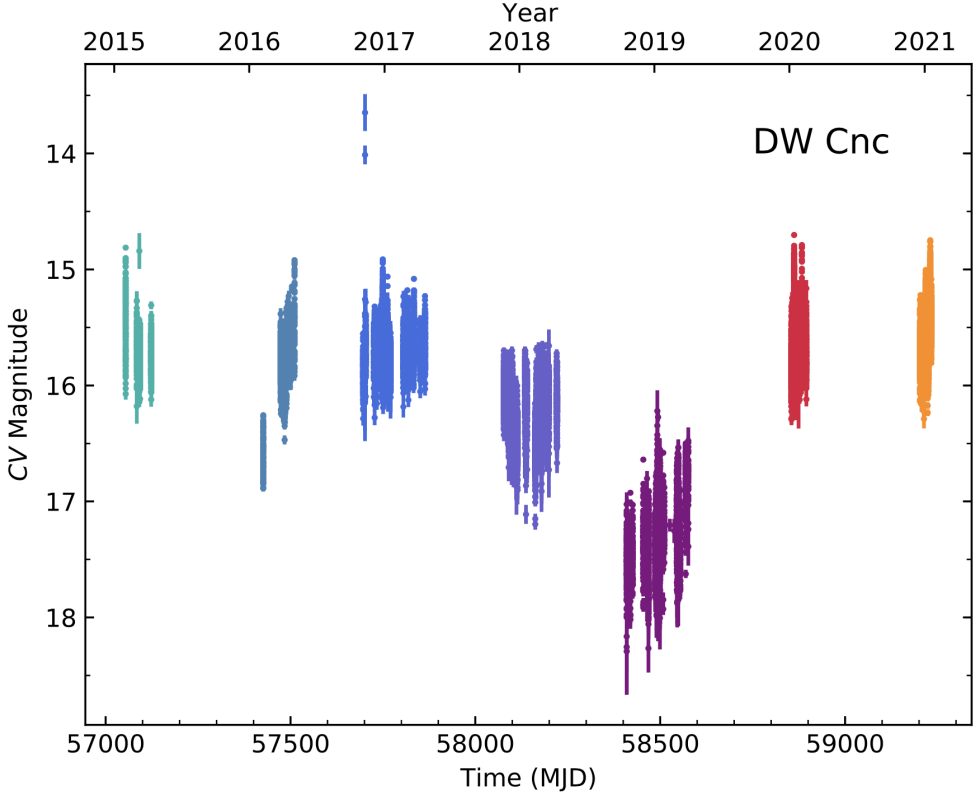


Figure 4: AAVSO light curve of DW Cnc from 2015–2021, (Covington et al., 2021)

However, these observations are generally of the visible spectrum as pointed X-ray observations are challenging to coordinate. As such, Dr. Aarran Shaw proposed that upon observations of a system entering a low state in the V-band filter, 50ks *XMM-Newton* space-based X-ray observations be made to study the accretion mechanisms at play closer to the WD (Shaw, 2021). To this effect, the Great Basin Observatory (GBO) is used to observe each of the 13 targets for this study in the V filter to determine optimal timing for further X-ray observations. In section 4 we present the pipeline used to calibrate and analyze the data, and in section 5 we analyze the efficacy of the pipeline and attempt to quantify the low states observed during the observational period.

4 Observation Setup

4.1 Targets

In this observation, the primary targets were 13 IPs (AO Psc, BG CMi, DO Dra, DW Cnc, FO Aqr, GK Per, PQ Gem, RX J2133.7+5107, V405 Aur, V515 And, V709 Cas, V1062 Tau, and V2306 Cyg). From observations made using the Great Basin Observatory (GBO), the magnitudes of the luminosities of these systems are generally comparable, ranging from 12-15 magnitudes to 15-17 magnitudes in the case of a periodic dip. Across these targets are 1600

existing data points with more being generated as observations occur, from March 2020 to April 2022. To handle this volume of data such that pointed X-ray observations can be triggered, an automated pipeline is required.

4.2 Differential photometry

Observations of the night sky require the use of “differential photometry,” a technique that uses existing knowledge of the brightness of light sources in the night sky to determine the relative brightness of a target star. Light from target stars hits a charge-coupled device (CCD), which effectively serves as a camera sensor and records pixel data as a 2D array of photons that hit the CCD. It stores these as “counts,” and can generally be thought of as the brightness of a given pixel. Unlike standard cameras, this data is recorded raw and uncompressed as each pixel contains vital data for observations. The resulting image is then calibrated against a flat field and dark frame to remove noise and biases resulting from the filter and/or the CCD itself. Once a calibrated image is formed, differential photometry can be performed. First, counts of a background area are taken as a baseline to be subtracted once counts of the stars are tallied. Generally, this is taken from a region of the image that is devoid of stars or from a ring around the aperture on each star called an annulus. Then the counts of the reference stars and the target star are taken and equation 4 is used to calculate the magnitude of the target star.

$$m_{star} = -2.5 \log\left(\frac{N_{star}}{N_{ref}}\right) + m_{ref} \quad (4)$$

Typically this will be performed over a number of reference stars of known magnitudes in the image taken, and the resulting magnitudes will be averaged. The uncertainty of the calculations is to be taken as the standard deviation across these magnitudes. An example of an image on which photometry would be performed can be seen in figure 5.

4.3 Relevant technologies

Visible spectrum observations of each of the targets are made using the GBO and the data is fed through Astrometry.net to append coordinate data before being deposited onto a Linux machine. Here, the data is calibrated and photometry is performed on each of the stars in question using Photometry+, a Python application built to make performing quick photometry easier (Tudor, 2020). Other Python libraries utilized in this project: Typer, to turn the program into a command-line utility; Astropy, for interacting with Flexible Image Transport System (FITS) files and headers; and Matplotlib for plotting the final program.

The data collected from the GBO is in the form of FITS. In addition to maintaining the raw image such that accurate photometry can be performed on targets, the FITS file format allows for much more information to be included with each data point. Relevant to this project, the FITS file format includes a header that includes the image type (light frame, dark frame, flat

field), the date of the observation in Julian Date format, the exposure time in seconds, and the coordinate data of the image.

4.4 Program

The program created for these observations was developed using Python, borrowing heavily from Photometry+. Though an extremely helpful application, Photometry+ is not very mature and as such comes with its share of bugs and errors. Compounded with the inconsistency of the data and that most of the design efforts focused on a graphical user interface instead of a module from which to be pulled, more thorough error handling and logging were required to handle the volume of data used in this project.

4.4.1 Program constants and directory structure

This program may require some configuration before it can be moved between machines. First, `photometry_app.py` contains several constants that must be updated to match the machine. The `CALIBRATION_PATH` and the Dark and Flat paths can be changed in tandem if necessary. Optionally, the location of the Astrometry.net API token and the location of the output folder can be changed. By default, outputs will be placed in `./Output/` and the API key will be searched for in `./token.txt`. When using the run script from this project, ensure that the `STAR_DIR` variable is accurate and that there is a file `Star_List.csv` with a table of the stars, their coordinates, as well as the size of the desired radius of the aperture (in pixels) to be applied to each star and its reference stars. Table 1 shows the `Star_List.csv` file used in this project. Note that if the names of the columns change then it must be reflected in `run_wcs.py`, and that this project used folders matching the names of the targets.

Table 1: A list of target stars for this project and their associated coordinates.

Source name	RA	Dec	Radius
AO Psc (V)	343.8249478316139	-03.1777688193433	27
BG CMi (V)	112.8708731255740	+09.9397242531953	27
DO Dra (V)	175.9103755737186	+71.6890413478491	27
DW Cnc (V)	119.7210059838655	+16.2792081192554	27
FO Aqr (V)	334.4807542571472	-08.3510384935365	27
GK Per (V)	052.8000517768417	+43.9042936391586	27
PQ Gem (V)	117.8222057627658	+14.7399592149954	27
RX J2133.7+5107 (V)	323.4318215913692	+51.1235414964274	27
V405 Aur (V)	089.4970656680238	+53.8958071792211	27
V515 And (V)	013.8327340186671	+46.2158311392901	27
V709 Cas (V)	007.2034613661951	+59.2894553692881	27
V1062 Tau (V)	075.6145003691148	+24.7564277766907	27
V2306 Cyg (V)	299.5602955767195	+32.5450066716087	27

4.4.2 Indexing directories index_dir

Example function call:

```
index_dir(path='path/to/dir', clean_run=True)
```

This will generate an index file at path/to/dir/index.csv that contains relevant information on the contents of the directory. This includes the modified Julian date (MJD), image type (light frame, flat field, dark frame), exposure time in seconds, coordinate data (true/false), the filter type (typically V in this project), and whether or not photometry has been performed on the file. To analyze data, we first need to know the background from which it comes. Since FITS files contain much of this background information in their headers, this is relatively simple as the Astropy Python library contains a module for opening and reading FITS files and their headers. However, when performing photometry on many files at once, opening and reading each one will dramatically slow down the program. The solution to this is simple: read each file once, and then never again. By extracting all relevant header data to an index spreadsheet in each folder, the time it takes to obtain this information is cut down dramatically. As an added benefit, it also congregates the data for quick and easy viewing and serves as a central location to put additional information on each data point including its file path and whether or not photometry has yet been performed on it.

Generally, this function is used only once - either manually through the command-line utility or automatically when the photometry function does not detect an index file in the containing folder of a data point.

4.4.3 Finding the best calibration files find_dark and find_flat

Example function call:

```
find_dark(input_file='path/to/fits/datapoint')
```

When performing photometry on these data points, they must often be calibrated beforehand. The data from the GBO is usually calibrated using a flat field of a matching filter type and a dark frame of a matching exposure time to the data instead of using a bias frame. Using the index file in the containing folder, this function will find the best calibration file available. For flat fields, it matches date and filter type and for dark frames, it matches exposure time and date.

4.4.4 Photometry Function run_photometry

Example function call:

```
run_photometry(target_RA, target_DEC, 'path/to/target/file.fits', save=True)
```

This will use `index_dir` along with `find_flat` and `find_dark` to find the best calibration files to calibrate the data. Then, it will perform photometry on the target star and output a list of reference stars as a CSV file. It will then (assuming no errors) update the `index.csv` file for the target file's directory to show that it has been run. If `save=False` is picked, it will not update this directory and instead will just output the information found. If the program runs into an error, this is logged and the program continues running. This function is responsible for producing the actual data output. If necessary, it will use the previous auxiliary functions to index the directory to find the proper calibration files and then perform photometry on the given FITS file. The actual photometry is primarily handled by Photometry+, so this function serves two primary purposes. The first is proper logging - Photometry+ has many unhandled errors that will disrupt bulk photometry runs, it is important to note these (and fix them if possible), but then move on. The second is data handling, it provides a much more standardized manner of returning information (including auxiliary data, such as reference stars used) and it will update the index file with whether or not it has been run.

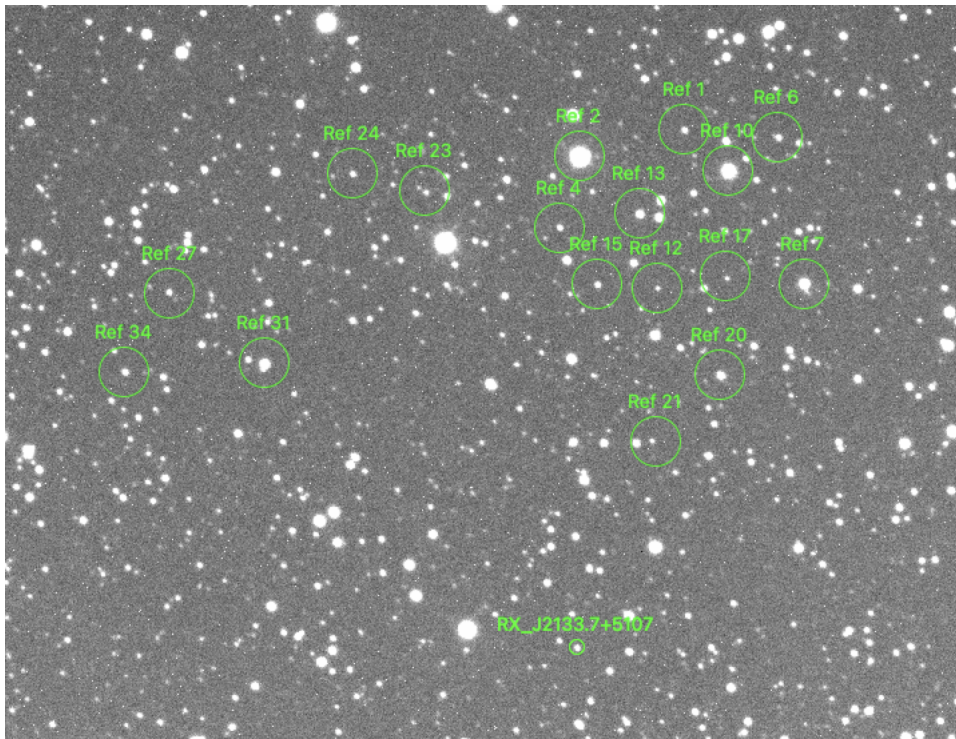


Figure 5: An image of the RX J2133.7+5107 field, with the star and selected reference stars labeled.

4.4.5 Plotting `plot_light_curve`

Example function call:

```
plot_light_curve(  
    input_file='path/to/output/output.csv', output_file=None, title=None
```

)

This function will create a graph of the data found in `output.csv` plotting date (MJD and standard) versus magnitude, generating the output file name and title automatically from the input file name if none is given, with the most recent data point highlighted in red. See fig 6 for an example output of this function. In addition, this function has the responsibility of dropping extraneous data points by dropping all data points with an absolute error higher than 0.3. Though the data is saved in case it is required for more detailed analysis, it is not useful to include on the graph as it may change the scaling and in effect hide the desired information.

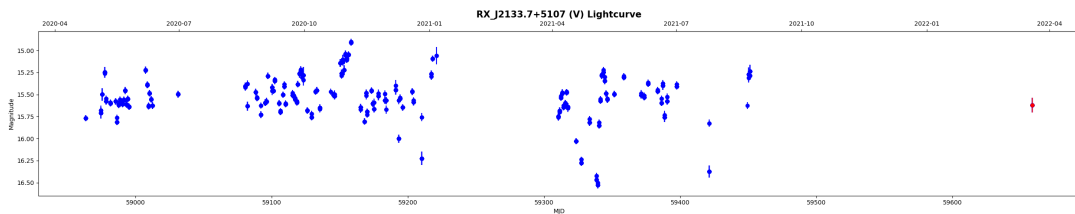


Figure 6: Example output for RX J2133.7+5107

4.4.6 Cron job and Run Script

As the primary application is written as a command-line utility, an automated pipeline would require a run script to call the functions at regular intervals. The run script for this application is called once per day and outputs logs into a file labeled with the date of the execution and includes all notices, warnings, and errors that are generated by the code. This allows the program to continue running even after encountering substantial issues on a data point while recording the issues and their underlying causes. The run script will call the primary application to perform photometry on any new or novel data points; update index files; generate plots; and move all logs, index files, and plots into a Dropbox folder to be viewed as necessary. When adapting this program for further use, this run script may be made or another one may be substituted without any issues. For logging, it is recommended to separate by each execution or each day as the standard output and standard error can build up substantially over the lifetime of the program.

5 Results

5.1 Data

In this project, 1,666 data points have been run, and 1,303 of them already had coordinate data. Of the 1,303 data points with coordinate data, 1,277 were run at a success rate of 96%. Of the 363 data points without coordinate data, 303 of them have had coordinate data affixed but only

26 of them were run at a success rate of 7%. Overall, the success rate was 77% across all of the 1,666 data points. For a full breakdown of this distribution across the target stars, see table 2.

Table 2: Information on each of the stars for how many data points were run. WCS refers to the presence of a world coordinate system for the data point.

Target Star	Total Count	WCS %	Ran %	WCS Ran %
V2306 Cyg	186	91%	89%	97%
V709 Cas	161	81%	80%	98%
V515 And	137	64%	59%	93%
V405 Aur	151	91%	89%	99%
RX J2133 7+5107	167	83%	81%	98%
PQ Gem	118	73%	72%	99%
GK Per	135	87%	86%	98%
FO Aqr	124	74%	69%	93%
DO Dra	289	66%	60%	91%
BG CMi	75	91%	91%	100%
AO Psc	123	69%	85%	93%
Summary	1666	78%	77%	96%

5.2 Analysis

Further inspection of failed data points reveals that they appear to generally have various malformations. Some appear overexposed, some have large disruptions to the image, and many have “trails” as a result of the rotation of the earth not matching the motion of the telescope. An example of such a disruption can be seen in fig 7. As the GBO will make API calls to Astrometry.net to affix coordinate data to its observations, it follows that data points without coordinate data have failed when making the API call. This explains the high failure rate among those data points. Despite these failures, many of these data points are successfully calculated but do not meet the error cutoff of the program due to artifacts or other issues with the image. Consequently, these are not included in the plot.

To validate the data, figure 6 can be compared to data from the ASAS-SN telescope in the g filter as seen in figure 8. Here, the dips in both data sets match very closely. This lends credence to the use of the GBO as an instrument to determine the presence of a low state of an IP. From inspection of the resulting plots across all targets, between March 2020 and April 2022 there were 9 dips corresponding to low states among the targets. See Appendix A for the annotated plots. There are some time ranges among the plots where a dip is present but is not annotated on the plot - this is because there is not enough data or the data present is not good enough to confidently assert that it is a low state of the IP. On the other hand, more recent data has a lower error and consequently a higher level of confidence. Therefore, the dip is annotated and counted as a low state despite fewer data points (as seen in the light curve for DO Dra).

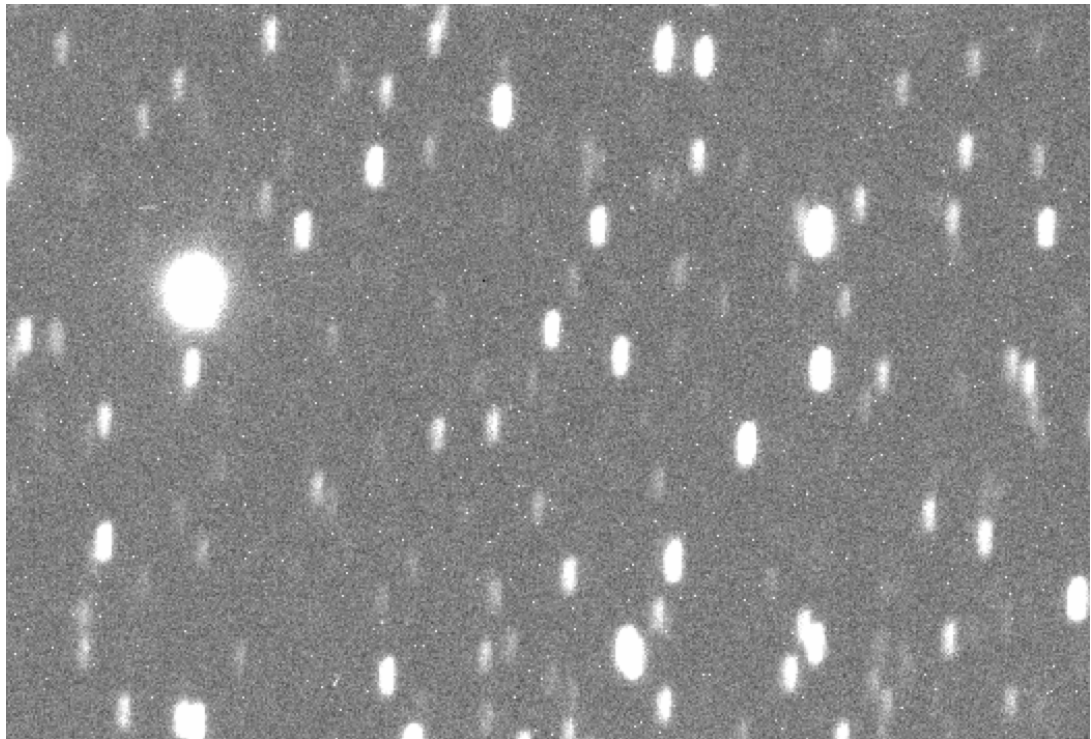


Figure 7: A snapshot of trails in an image taken from the Great Basin Observatory.

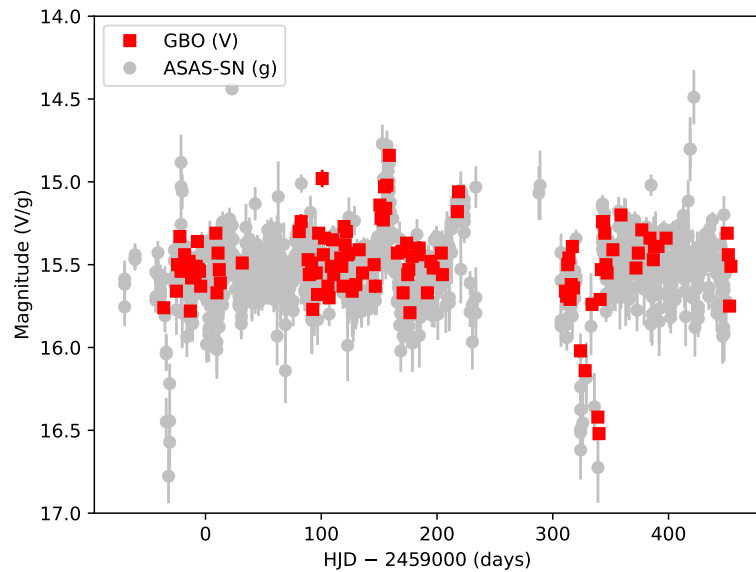


Figure 8: GBO data and ASAS-SN data of RX J2133 7+5107 between 4/21 and 6/21

5.3 Summary and Conclusions

Though functional, the automated pipeline created for this project is far from complete. In fact, it is designed to become obsolete. Many, if not all of the features of this program, can be built into Photometry+ and used to help it mature into a more robust application as well

as a library from which to be pulled for scripts like those used in this project. So, the future of this program is to be absorbed into Photometry+ and for improvements to be made on that application - namely, more robust error handling and logging and packaging of the program for simpler installation and utilization in future projects (similar to this one). In addition, many improvements could be made to the algorithms present in Photometry+. Photometry+'s API calls to Astrometry.net are the largest time sink at times taking up to five minutes, often without much success. Instead of uploading the entire image, times could be drastically reduced if the information on the stars present in the FITS image is taken and sent to Astrometry.net directly instead. Though Photometry+ already uses annuli around the aperture to determine background counts for the target star and reference stars, the choice of size of the aperture itself could be further matured to automatically determine if three times the full half-width maximum is the best radius (as it generally is) or if the field is too crowded and a custom radius needs to be generated. Finally, in Photometry+ the aperture is centered exactly where the input coordinates are, and though close, it should include a centering algorithm to place the center of the aperture at the center of flux around the star.

Understanding IPs, and more fundamentally WDs, serves to be a foundational area of cosmology as it advances. Automated pipelines, designed to remove monotony and drudgery from analyzing data, help to propel the field forward by further abstracting the work required for such observations. By automating tasks, focus can remain on the observations that matter. In the case of this program, so far it has shown 9 dips across the 13 targets considered over a two-year span. That the pipeline was able to produce these results despite gaps in observations and volatility among the data, is a testament to the utility that such automation can provide to cosmology.

References

- Covington, A. E., Shaw, A. W., Mukai, K., & Littlefield, C. (2021). Investigating the low-flux states in six intermediate polars.
- Falanga, M., de Martino, D., Bernardini, F., & Mukai, K. (2018). Magnetic cataclysmic variables discovered in hard x-rays. *1*.
- Hailey, C. J., Mori, K., Perez, K., & Canipe, A. M. (2016). Evidence for intermediate polars as the origin of the galactic center hard x-ray emission.
- Laboratory, L. B. N. (2014). Standard-candle supernovae are still standard, but why? <https://astronomy.com/news/2014/03/standard-candle-supernovae-are-still-standard-but-why>
- Maoz, D. (2016). *Astrophysics in a nutshell* (2nd ed.). Princeton University Press.
- Shaw, A. W. (2021). Investigating accretion in the rare low-flux states of intermediate polars.
- Suleimanov, V. F., Doroshenko, V., & Werner, K. (2019). Hard x-ray view on intermediate polars in the gaia era.

Tudor, A. R. (2020). *Photometry+*. <https://github.com/Alexandara/photometry-plus>
 Williams, D. R. (n.d.). Sun fact sheet. <https://nssdc.gsfc.nasa.gov/planetary/factsheet/sunfact.html>

6 Appendix A: Annotated plots

